Machine learning-based monitoring of war-damaged water bodies in Ukraine using satellite images

Kateryna Sergieieva[1,*,†], Olena Kavats[2,†], Volodymyr Vasyliev[3,†], Yurii Kavats[2,†] and Oleksandr Kovrov[1,†]

[1] *Dnipro University of Technology, av. Dmytra Yavornytskoho 19, 49005 Dnipro, Ukraine*
[2] *Ukrainian State University of Science and Technology, av. Nauky 4, 49600 Dnipro, Ukraine*
[3] *National University of Water and Environmental Engineering, st. Soborna 11, 33028 Rivne, Ukraine*

Abstract

Water resources are Ukraine's strategic environmental asset. As a result of the destruction caused by the Russo-Ukrainian War, critical water infrastructure has been severely damaged. This makes it essential to effectively manage and conserve water resources in the face of increasing anthropogenic impact. The use of machine learning methods to monitor water bodies' conditions based on optical and Synthetic Aperture Radar (SAR) satellite images allows for automating analysis processes and providing more accurate and timely results, which is important for making reasonable management decisions. In this study, information tools for mapping and assessing the dynamics of surface water body changes were developed based on Sentinel-1 and Sentinel-2 data using a convolutional neural network. They were used for the mapping of surface water bodies in the Lower Dnipro sub-basin affected by the destruction of the Kakhovka Hydropower Plant dam. To improve the result of satellite image mixed pixels classification in shallow areas of swampy water bodies at the bottom of the destroyed Kakhovka Reservoir, it is proposed to use a block data model and a probabilistic approach to assess the presence of "water" and "ground" class objects in the images, which allows to achieve mapping accuracy of up to 96%.

Keywords

machine learning, convolution neural network, block model, Sentinel-1, Sentinel-2, water

1. Introduction

Surface water resources play a key role in the functioning of human society and ecosystems worldwide [1]. In Ukraine, water bodies are increasingly threatened by pollution and degradation as a result of military operations and unsustainable management practices and require the introduction of modern information technologies to detect changes in their condition in a timely manner and to support management decisions.

According to the Water Code of Ukraine, the Law of Ukraine on Environmental Protection, the Water Strategy of Ukraine until 2050 and other legislative acts, all water resources are subject to protection from pollution, contamination, depletion and other impacts that may affect water supply conditions, harm human health, reduce fish stocks, worsen the living conditions of some animals, reduce soil fertility and other adverse effects due to changes in the physical and chemical properties of water, reduce its capacity for natural purification and disrupt the hydrological and hydrogeological regime. The Russian invasion of Ukraine caused significant and sometimes irreparable damage to the critical infrastructure of centralized water supply and sewerage, hydrotechnical structures for flood control, as well as hydropower facilities and the hydrotechnical

[1] *ICST-2024: Information Control Systems & Technologies, September , 23 – 25, 2024, Odesa, Ukraine*
* *Corresponding author.*
† *These authors contributed equally.*
sergieieva.k.l@nmu.one (K. Sergieieva); alena.kavats@gmail.com (O. Kavats); v.v.vasiliev@nuwm.edu.ua (V. Vasyliev); yukavats@gmail.com (Yu. Kavats); kovrov.o.s@nmu.one (O. Kovrov)
0000-0001-7345-2209 (K. Sergieieva); 0000-0002-0172-7856 (O. Kavats); 0000-0002-5211-9164 (V. Vasyliev); 0000-0002-0180-5957 (Yu. Kavats); 0000-0003-3364-119X (O. Kovrov)

network of irrigation and drainage systems. The Association Agreement between Ukraine and the EU requires Ukraine to implement the provisions of Directive 2000/60/EC (Water Framework Directive) [2]. It requires Member States to take the necessary measures to prevent the deterioration of all surface water bodies [3]. According to the Association Agreement with the EU, Ukraine must also implement relevant measures in practice [4].

Due to the destruction of ground-based monitoring stations as a result of military operations, satellite imagery is the main source of data on the surface water bodies condition. Water bodies are characterized by enhanced absorption of solar radiation in the optical, near and shortwave infrared regions of the electromagnetic spectrum and are clearly distinguished from other classes of the Earth's surface by their low reflectance values [5, 6]. Among the freely available optical satellite images, the best spatial resolution of 10 and 20 m and the highest revisit frequency (5 days in the absence of cloud cover) are provided by the Sentinel-2 satellites of the European Commission's Copernicus Earth Observation Programme implemented in partnership with the European Space Agency. Images can be downloaded from the EO Browser (https://apps.sentinel-hub.com/eo-browser), Copernicus Browser (https://browser.dataspace.copernicus.eu/), Alaska Vertex (https://search.asf.alaska.edu/), etc. platforms. Sentinel-2 spectral bands and spectral indices calculated from them, such as Normalised Difference Water Index (NDWI), Modified Normalised Difference Water Index (MNDWI), Automated Water Extraction Index (AWEI), etc. are input data for surface water body classification and identification tasks [7, 8].

Synthetic Aperture Radar (SAR) satellite observations allow the dynamics of water surface changes to be monitored regularly and independently of weather conditions. The interaction of the radar signal with the surface is characterized by the backscatter ratio (σ^0), the value of which depends on surface properties, in particular relief, texture, moisture and surface conductivity [9]. Since a smooth water surface is a specular reflector, a significant portion of the reflected signal does not reach the radar sensor, so water objects are characterized by a very low backscatter value and are represented by a dark color in SAR images [10]. The freely available Sentinel-1A Ground Range Detected (GRD) SAR images (Sentinel-1B has been decommissioned in December 2021) at a spatial resolution of 10 meters and a revisit frequency of 12 days allow regular all-weather monitoring of surface water bodies.

The simplest approach to surface water mapping is threshold segmentation. The "water" class includes Sentinel-2 pixels with positive NDWI and MNDWI values [11]. In the case of SAR data, water bodies are distinguished from objects with other backscattering by selecting the σ^0 threshold, e.g. using the Otsu method based on the σ^0 histogram and its approximation by Gaussian or gamma distributions [12]. The optimal threshold can be determined based on the principle of maximum similarity of the resulting water mask obtained from SAR data to the reference mask [13]. In this case, the maximum accuracy of the result is achieved for the data in VH polarization, and the data in VV polarization are the most resistant to threshold variations [14]. However, such approaches have not been sufficiently studied in areas of waterlogged soils and wetlands, which are characterized by the presence of mixed pixels in the images. In this situation, it is preferable to use a probabilistic approach and machine learning methods.

Machine learning approaches are widely used in the mapping of water bodies [15]. Convolutional Neural Networks (CNN) provide high accuracy results, provided a representative sample of reference areas of the Earth's surface is available [16]. Algorithms such as decision trees, random forests and support vector machines have proven highly effective in detecting pollution and predicting water quality [17]. Linear regression, decision tree regression and multivariate regression help to predict quantitative indicators such as the level of pollution or the concentration of certain chemicals in water [18]. K-means, hierarchical clustering and DBSCAN algorithms allow water bodies to be grouped by similarity of condition, helping to identify areas with similar environmental characteristics [19].

The peculiarity of mapping the water surface of hydrotechnical facilities destroyed by war is the presence of numerous shallow water bodies or swampy areas, which produce mixed pixels on satellite images and cause an additional error in the mapping results. Shallow surfaces can be misclassified as

ground, contributing to inaccuracies in water mapping. This requires finding new classifiers capable of correctly separating mixed classes.

Therefore, the aim of this study is to develop new information tools for the mapping of surface water bodies, based on machine learning methods, which will also ensure the correct detection of pixels of the "water" class in swampy areas.

2. Materials and Methods

2.1. Study area

The study area of about 8 thousand km^2 is located in southern Ukraine at the intersection of Dnipropetrovsk, Kherson and Zaporizhzhia Oblasts, and includes a fragment of the Lower Dnipro Basin, the Dnipro, Tomakivka, Solona, Kinska, and Kamianka rivers, Belozersky Liman, the Zaporizhzhia Nuclear Power Plant (ZNPP) pond and the Kakhovka Reservoir, destroyed by the occupiers as a result of the Kakhovka Hydroelectric Power Plant (HPP) dam collapse during the Russian invasion of Ukraine on 6 June 2023 (Fig. 1).

The dam's explosion caused a rapid water outflow from the Reservoir. Before the disaster, its area was about 2.2 thousand km², and by 11 June 2023, the water level in the Reservoir had dropped by 73%.

The destruction resulted in the creation of 5-8 large reservoirs connected by the old Dnipro riverbed, and 15-20 medium and large reservoirs that lost their direct connection to the river [20]. The irrigation and drinking water supply systems in both the occupied and Ukraine-controlled territories were destroyed.

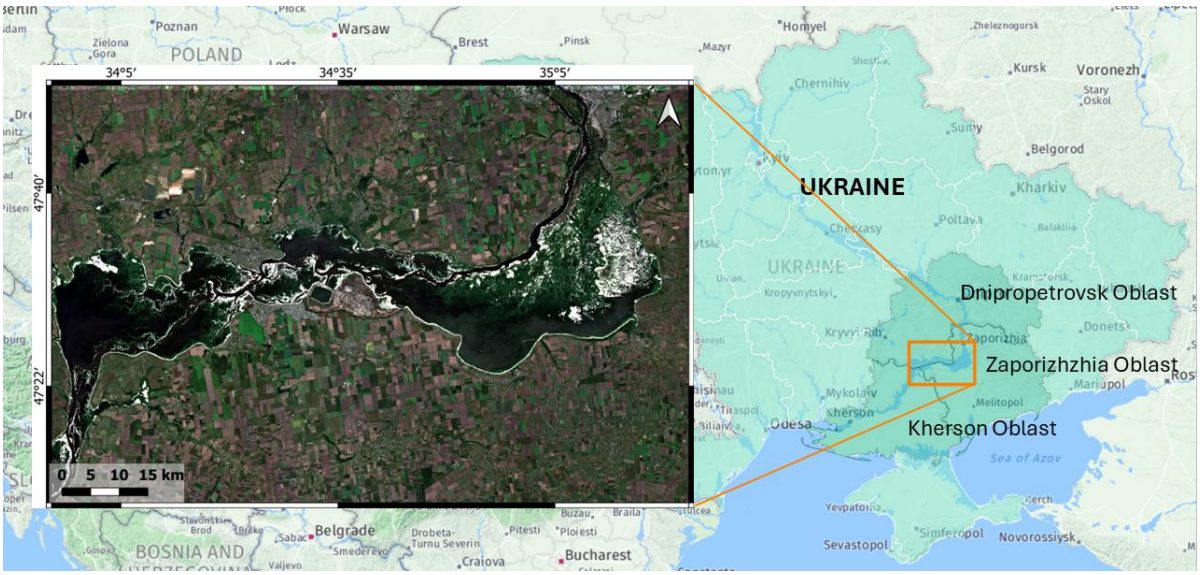

Figure 1: Study area in Dnipropetrovsk, Zaporizhzhia and Kherson Oblasts of Ukraine. Sentinel-2 image, 25 May 2024. Basemap: Here Wego Terrain (EPSG:4326–WGS 84).

2.2. Satellite data

Cloud-free Sentinel-2 images and Sentinel-1 images close in acquisition time were used as input data for surface water detection.

Three observation periods were selected: before the Kakhovka HPP dam collapse, two weeks and one year after the collapse.

The observation periods were chosen at a time when the water surface of the Kakhovka Reservoir was not changing too rapidly, allowing the joint use of Sentinel-1 and Sentinel-2 images with a slight time lag. Satellite image acquisition dates are shown in Table 1.

Table 1
Sentinel-1 and Sentinel-2 image acquisition dates

Observation period	Satellite	Acquisition date
Before dam collapse	Sentinel-1	03.05.2023
	Sentinel-2	06.05.2023
Two weeks after dam collapse	Sentinel-1	20.06.2023
	Sentinel-2	20.06.2023
One year after dam collapse	Sentinel-1	21.05.2024
	Sentinel-2	25.05.2024

Sentinel-2 L2A images resulting from atmospheric correction contain Bottom of Atmosphere (BOA) reflectance were taken from the Copernicus Open Access Hub (https://scihub.copernicus.eu). Bands "B02" (490 nm), "B03" (560 nm), "B04" (665 nm), "B05" (705 nm), "B08" (842 nm), "B11" (1610 nm) were used in each acquisition date.

Sentinel-1A GRD Interferometric Wide (IW) images were acquired from Path 167: Flight Direction — Descending, Frames — 431, 437. The Sentinel-1 GRD datasets were converted to SAR backscattering coefficient σ0. Images were pre-processed using ESA SNAP 8.0 software (https://step.esa.int/) in the following main stages [14, 21]: Apply Orbit File, Remove Thermal Noise, Remove GRD Border Noise, Calibration, Speckle Filtering, Terrain Correction (Copernicus 30 m Global DEM), Linear-to-dB.

2.3. Water Body Detection Methods

2.3.1. Convolutional neural network

Satellite images were classified using a CNN with a logistic activation function, using the Adaptive Moment Estimation (Adam) Optimizer and the categorical cross-entropy loss function [22]. The neural network architecture consists of three convolutional layers, each accompanied by a dimensionality reduction layer followed by a layer that converts 2D data to 1D and two fully connected layers.

The neural network model is implemented in two ways: using the Keras library (Python programming language) and using ML.Net (C# programming language) [23].

2.3.2. Block data model

Some fragments of the input images contain swampy areas at the bottom of the destroyed Kakhovka Reservoir, which are either shallow water or wet soil, and can be classified as "ground" or "water" with almost equal probability. This factor adds uncertainty to the model and reduces the accuracy of the binary classification. To improve the classification accuracy of mixed pixels, a physical data model is proposed that divides the input image into blocks and estimates the homogeneity of each block and its belonging to the "water" or "ground" class (Fig. 2). The combination of mowing scanning area method and binary CNN classification allows to obtain statistical characteristics for two classes ("ground" and "water") within mixed image fragments (blocks).

The model combines the following operations [24]:

1. Analysis of standard deviations and average values: for mixed blocks, the standard deviations and averages of the reflectance and σ^0 of the pixels are calculated for both classes. This allows to determine which class dominates in the image block.
2. Splitting into sub-blocks: significantly heterogeneous blocks can be split into sub-blocks for more detailed analysis. Each sub-block is classified again.
3. Analyzing of adjacent blocks:

- Scanning with a mowing window: the scanning window is shifted by half a block to analyze neighboring blocks. This allows to get additional information about the change in characteristics in adjacent areas and better understand their class distribution.
- Detection of blocks with a predominant class: after scanning, it is possible find blocks where, for example, ground predominates. To do this, we analyze the statistical characteristics of the blocks and determine which of them have a significant probability for one of the classes.
- Calculation of statistical characteristics: for each block, statistical characteristics (mean value, standard deviation) are calculated for pixels of "ground" class. Similar calculation is performed for blocks with a predominance of "water" class. This allows to obtain statistical characteristics for two classes within one disputed block.

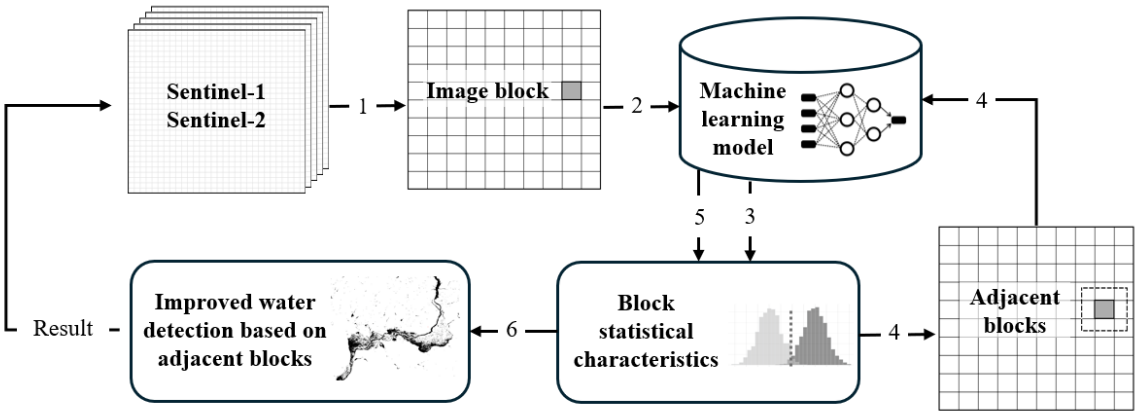

Figure 2: Physical data model in a surface water body mapping system.

The statistical characteristics obtained allow a more accurate classification of disputed blocks. If the probabilities for both classes in a disputed block are similar, additional statistical data can be used to make a final decision as to whether the block belongs in one class or another.

2.3.3. Classification accuracy assessment

Binary raster water masks are groups of adjacent or separate pixels that represent water bodies on the Earth's surface.

True Positive (TP), True Negative (TN), False Positive (FP) and False Negative (FN) indicators can be used to evaluate the effectiveness of the classification model in correctly and incorrectly identifying water bodies.

Binary similarity coefficients are measures of the similarity of two or more sets/objects by calculating the ratios of the combination and intersection of their elements or areas. In the case of water detection, the pixels of the class "water" of the resulting mask are compared with the water bodies of the reference mask. The Jaccard Index or Intersection-Over-Union (IoU) is a binary measure of similarity between the reference and the resulting water masks [14, 25]:

$$IoU = \frac{S_{B,R}}{S_B + S_R - S_{B,R}} = \frac{TP}{TP + FP + FN}, \quad (1)$$

where S_B — water bodies area on the reference mask,
S_R — water bodies area on the resulting mask,
$S_{B,R}$ — area of water bodies intersection on two masks.

IoU is calculated as the quotient of the intersection area of the reference and result masks divided by the area of their merging. Its value ranges from 0 to 1, where 0 means that the masks do not overlap and 1 means that the masks overlap completely.

The approach to statistical analysis of image blocks is more localized and specific to solving the problem when both classes are present in the block. It differs from IoU, which is used to evaluate the accuracy of object detection in general and does not include analysis of the behavior of neighboring areas or calculation of statistical characteristics of classes. IoU is used to assess the accuracy of the resulting water mask.

3. Results

3.1. Water bodies identification

To implement the neural network classification models, and the proposed block model of data representation and statistical analysis, information tools were developed using the .NET Framework platform. It consists of the following modules:

- Modelling: neural network models and their integration.
- Image processing: image upload, pre-processing and block representation using the OpenCV library.
- Classification: uses neural network models to classify and statistically analyze each image block, determining the probability of fragments belonging to different classes of "ground" and "water" and storing the results for further analysis.
- Visualization: is responsible for displaying the classification results on the original image, adding appropriate labels and indicators to the image fragments to clearly present the processing results to the user.

Figure 3 shows an example of an image block model. Each block is estimated to belong to the class "ground" (g) or "water" (w). The decision to belong to one or the other class is made based on the maximum probability given in the top line of each block label.

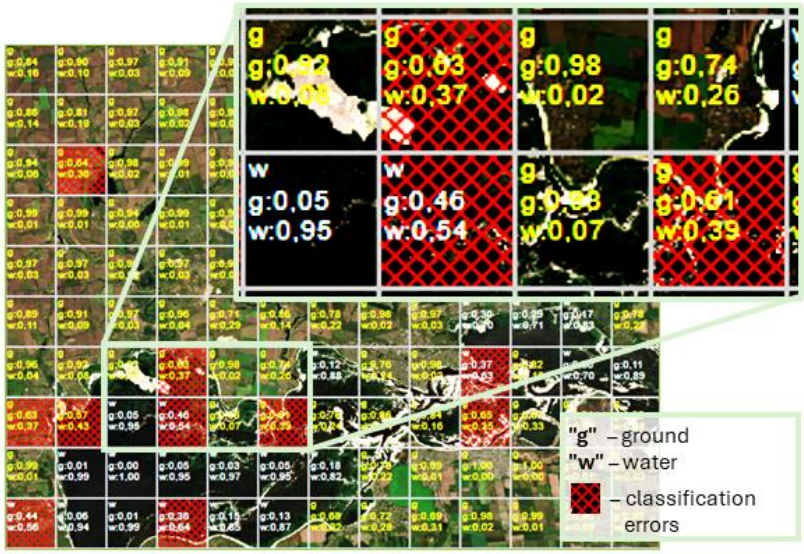

Figure 3: Estimation of the probability of image blocks belonging to the classes "ground" and "water". Base image: Sentinel-2 from 25 May 2024.

The red shading in Figure 3 shows misclassified blocks corresponding mainly to the coastal areas of the Kakhovka Reservoir with shallows and swamps. For such blocks, the homogeneity of the

classes was assessed by calculating the mean and standard deviation of the integral indicator, which is a combination of normalized input datasets (Fig. 4).

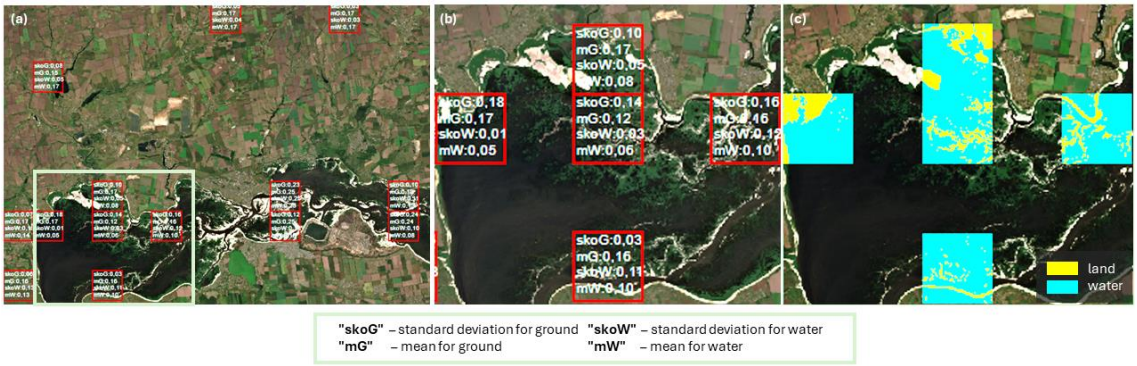

Figure 4: Estimation of the mean and standard deviation of the integral indicator for pixels of the classes "ground" and "water" in blocks with classification errors: (a) investigated area; (b) statistical characteristics of the distribution of classes within the blocks; (c) the resulting pixel-by-pixel classification of the analyzed blocks. Base image: Sentinel-2 Natural Colour, 25 May 2024.

Figure 5 shows an example of the estimated classification error for one of the image blocks. For this block, the CNN model estimated the probability of the ground to be 0.46 and the probability of the water to be 0.54.

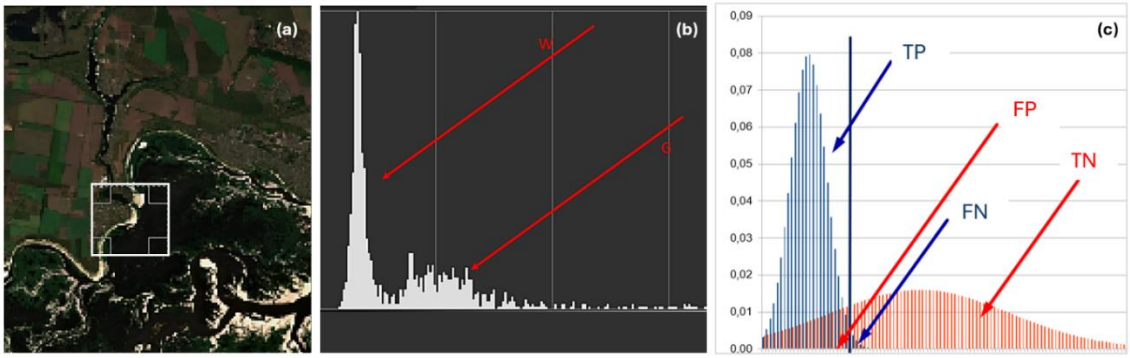

Figure 5: Distribution of the integral indicator in the image block of mixed pixels: (a) white color indicates the location of the analyzed image block; (b) bimodal histogram of the integral indicator value distribution; (c) histogram approximation by Gaussian distribution. Base image: Sentinel-2 Natural Colour, 25 May 2024.

Consider the frequency distribution of the integral indicator, which is a bimodal histogram, where the low-value mode corresponds to pixels of the "water" class (W), and the high value mode corresponds to pixels of the "ground" class (G) (Fig. 5b). The bimodal histogram for each class is approximated by a Gaussian distribution with the mean and standard deviation parameters determined empirically for the pixels of the corresponding classes of the analyzed image block (Fig. 5c), for example:

$$f(I_w) = \frac{1}{\sigma_w\sqrt{2\pi}} e^{-\frac{(I_w - m_w)^2}{2\sigma_w^2}}, \quad (2)$$

where I_w — pixels of the "water" class,
m_w — mean value determined empirically for the pixels of the "water" class,
σ_w — standard deviation value determined empirically for the pixels of the "water" class.

If the classes do not overlap, the threshold can be calculated based on the Otsu method using the local minimum of the bimodal histogram. In the case of overlapping classes, it is important to choose the correct threshold value to separate the "ground" and "water" classes. In our case, the threshold value was chosen according to the criterion of minimizing the first-order error, minimizing standard deviation within the "water" and "ground" classes and maximizing the TP indicator (Fig. 5c):

$$th_{\sigma^0} = argmin_{th_{\sigma^0} \in \Omega}(K(th_{\sigma^0})), \quad (3)$$

where $th_{\sigma^0} - \sigma^0$ threshold value,
$\Omega -$ the set of all permissible σ^0 thresholds,
$K(th_{\sigma^0}) -$ threshold selection criterion.

The statistical analysis for the selected image block estimated the probability of correct detection of water areas TP=0.99, probability of error FP=0.17 (probability of classifying ground as water), probability of missing water FN=0.01, IoU=0.846. This indicates a significant improvement in classification accuracy compared to the initial results of the neural network model (Fig. 3).

To visually assess the result, a binary classification was performed for the selected heterogeneous blocks (Fig. 4c), for which statistical analysis was applied to improve the class separability. Visual analysis of Figure 4c shows that the classification result is consistent with the Sentinel-2 base image. The ground contours are clearly visible in the classified image, demonstrating the accuracy of the method.

3.2. Monitoring changes in the water surface area

The dynamics of water surface changes in the study area is analyzed. Figure 6 shows the multi-temporal water masks generated using the information tools proposed in this paper.

Before the destruction of the Kakhovka HPP dam, the estimated water surface area over investigated site (Fig. 6a) was maximum and amounted to 23% of the image fragment area (about 1.8 thousand km^2). It includes the area of the Kakhovka Reservoir and adjacent water bodies. Shortly after the dam's destruction (Fig. 6b), in June 2023 the percentage of water surface decreased to 11.2% (about 900 km^2) and in May 2024 was 8.8% (about 700 km^2) (Fig. 6c). According to ground-based observations, it is known that before the destruction, the total surface area of the Kakhovka Reservoir was 2155 km^2 (the length of the reservoir was 230 km, and the maximum width was 25 km) [26]. Two months after the dam breach, the area of the fragmented Dnipro riverbed was about 120 km^2; isolated shallow water bodies covered about 307 km^2, but continue to decrease due to evaporation and drainage, so it is unlikely that any aquatic bioresources will be preserved there [27, 28].

Figure 6: Multi-temporal surface water masks generated using the information tools proposed in this study: (a) before Kakhovka HPP dam collapse on 3 and 6 May 2023. Base image: Sentinel-2 Natural Colour acquired on 06 May 2023; (b) shortly after Kakhovka HPP dam collapse on 20 June 2023. Base image: Sentinel-2 Natural Colour from 20 June 2023; (c) one year after Kakhovka HPP dam collapse on 21 and 25 May 2024. Base image: Sentinel-2 Natural Colour from 25 May 2024.

Hence, the study results confirm the importance and effectiveness of applying modern machine learning methods to assess water bodies' state for their management. The use of these methods is critical for ensuring sustainable development and preserving ecological balance in Ukraine.

4. Discussion

4.1. Influence of Sentinel-1 flight direction

The appearance of water bodies on SAR images depends on the orientation of the Earth's surface and objects adjacent to water bodies relative to the direction and incidence angle of radar signal.

Depending on the flight direction (ascending, descending) and the incidence angle, radar shadows may appear or disappear on the image, and the nature of wave scattering may change, especially at water/forest and water/artificial object boundaries. Gulácsi and Kovács [29] compared the results of mapping water bodies using ascending and descending orbit data and concluded that there was no significant difference in the results. Kavats et. al [14] investigated the effect of the flight direction and confirmed the conclusion that there was no significant difference in the area of water bodies for ascending and descending orbits. Irrespective of flight direction, the water masks contain correctly highlighted water surfaces. Depending on the incidence angle of the radar signal, the radar shadow area includes various areas of the Earth's surface slopes, which can be misinterpreted as water bodies. The water masks for the different orbits contain different percentages of noise in vegetation areas and show some differences in the texture of gaps in water areas, but these do not affect the final mapping result.

4.2. Comparison with Otsu method

The proposed information tools for mapping surface water bodies were compared with existing methods, namely, SAR water masks generated by the Otsu method based on Sentinel-1 backscattering coefficient data in VH and VV polarization and optical water masks based on the NDWI spectral index from Sentinel-2 data (Fig. 7) [14]:

$$NDWI = \frac{(\rho_{Green} - \rho_{NIR})}{(\rho_{Green} + \rho_{NIR})}, \quad (4)$$

where ρ_{Green} and ρ_{NIR}— reflectance in the green or NIR spectral region.

The analysis was performed for the Zaporizhzhia NPP cooling pond, Bilozersky Liman, and the Dnipro River near the southern part of Zaporizhzhia, which are well visualized on satellite optical images and do not contain mixed pixels. We used the survey date of 20 June 2023, shortly after the Kakhovka HPP dam collapse, for which optical and SAR images are available, allowing for a reliable comparison. The reference water surface mask was created based on the visual interpretation of the Sentinel-2 Natural Colour image. The metric of correspondence between the reference and the resulting water masks was IoU.

Water mask based on NDWI data (Fig. 7b) shows the presence of water in the areas of the Zaporizhzhia NPP cooling pond, Bilozersky Liman, the main Dnipro riverbed and the full-flow areas of small rivers. The "water" class also includes pixel values close to zero for open ground and artificial surfaces in residential areas. There are many missing "water" class pixels in the main Dnipro riverbed and small swampy areas at the bottom of the destroyed Kakhovka Reservoir. The mask IoU accuracy is 0.876.

SAR water mask (Fig. 7d) obtained by the Otsu method with a threshold of σ^0 VV -18.1 dB is characterized by a smaller number of water pixel gaps in the areas of the main water bodies and shallow swampy areas at the bottom of the Kakhovka Reservoir, but such gaps are still present at the water/ground boundary. There are gaps in the water class pixels, for example, on the surface of the Mykolaiv Reservoir. At the same time, the disadvantage of SAR data is the presence of speckle noise on agricultural fields, slopes of ravine structures, and the sides of the Hrushevsky open pit.

The percentage of speckle noise in a SAR image depends on the type and size of the filter kernel, which is the subject of a further study. The mask IoU accuracy is 0.843.

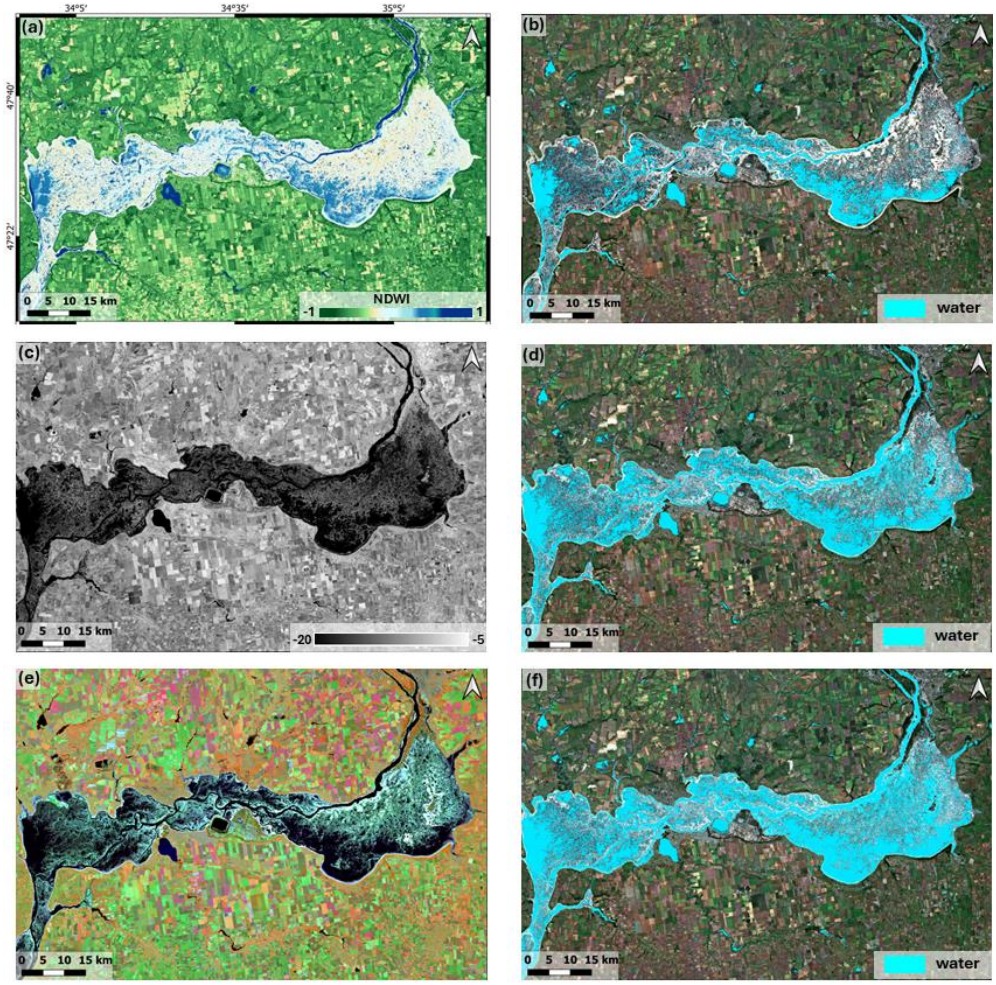

Figure 7: Comparison of surface water mapping results using different methods based on Sentinel-1 and Sentinel-2 data from 20 June 2023: (a) NDWI map; (b) water mask generated from positive NDWI values; (c) backscattering coefficient in VV polarization; (d) SAR water mask generated from σ^0 VV using threshold determined by the Otsu method; (e) pseudo-colour synthesis of Sentinel-2 bands B8-B11-B3; (f) water mask generated using the tools proposed in this study. Base image: Sentinel-2 Natural Colour, 25 May 2024.

The surface water mask generated by the information tools developed in this study, which is based on neural network classification and statistical analysis of image blocks, is characterized by the lowest number of data gaps on the water surface (Fig. 7f). At the same time, there are some misclassified water pixels in the ground areas. The mask IoU accuracy is 0.961, confirming the advantage of the proposed information tools over existing methods.

5. Conclusions

Novel approach to mapping surface water from SAR data is proposed. It is based on machine learning methods and a block physical data model, allowing to study statistical characteristics for two classes ("ground" and "water") within disputed image fragments. Information tools for mapping surface water bodies are proposed and developed using convolution neural networks, which includes the functionality of analyzing classification errors based on the assessment of the probability of correct detection of the "water" class pixels in swampy areas. Their peculiarity is the use of a block data

model and the analysis of the distribution of the "soil" and "water" classes within each block, which makes it possible to increase their separability based on the principle of minimizing the type I error.

The water masks generated by the proposed tools outperform the optical and SAR masks generated by thresholding methods based on the NDWI spectral index and the Otsu method. The resulting IoU accuracy of 0.961 indicates the applicability of this approach and the possibility of obtaining a reliable result.

The information tools can be easily adapted to changes in the input dataset and the number of classes. The practical significance of the results consists in the possibility of detecting problems in a timely manner and taking the necessary measures to solve them by integrating machine learning into the processes of monitoring and managing water resources. Additional opportunities may arise from the use of effective speckle noise filtering methods, which could also reduce the Type II error.

Acknowledgements

This study was funded by Ministry of Education and Science of Ukraine under the research work "The development of environmentally safe technologies for the restoration of man-made degraded territories in the conditions of post-war reconstruction" (0124U000357).

The authors would like to thank the European Commission, the European Space Agency, and the Copernicus Program for providing Sentinel data.

References

[1] R. Sabale, B. Venkatesh, M. Jose, Sustainable water resource management through conjunctive use of groundwater and surface water: A review, Innovative Infrastructure Solutions 8 (2023) 17. doi:10.1007/s41062-022-00992-9.

[2] A. Belokurov, C. Déchelette, M. Griffiths, G. Halpern, P. Seguin, A. Zinke, A shared water culture between the European Union and the Countries of the Eastern Neighbourhood, Water International 49 (2024) 563–571. doi:10.1080/02508060.2024.2321772.

[3] S. Wuijts, J. Claessens, L. Farrow, D. G. Doody, S. Klages, C. Christophoridis, S. Boekhold, Protection of drinking water resources from agricultural pressures: Effectiveness of EU regulations in the context of local realities, Journal of Environmental Management 287 (2021) 112270. doi:10.1016/j.jenvman.2021.112270.

[4] Association Agreement between the European Union and its Member States, Official Journal of the European Union, 2014. URL: https://eur-lex.europa.eu/legal-content/EN/ALL/?uri=CELEX%3A22014A0529%2801%29.

[5] M. K. Srivastava, S. Gaur, A. Ohri, P. K. Srivastava, N. Singh, Applications of remote sensing in water quality assessment, in: S. Lamine, P. K. Srivastava, A. Kayad, F. Muñoz-Arriola, P. C. Pandey (Eds.), Remote Sensing in Precision Agriculture, Academic Press, 2024, pp. 217–236. doi:10.1016/B978-0-323-91068-2.00019-9.

[6] G. E. Adjovu, H. Stephen, D. James, S. Ahmad, Measurement of Total Dissolved Solids and Total Suspended Solids in Water Systems: A Review of the Issues, Conventional, and Remote Sensing Techniques, Remote Sensing 15 (2023) 3534. doi:10.3390/rs15143534.

[7] J. Laonamsai, P. Julphunthong, T. Saprathet, B. Kimmany, T. Ganchanasuragit, P. Chomcheawchan, N. Tomun, Utilizing NDWI, MNDWI, SAVI, WRI, and AWEI for Estimating Erosion and Deposition in Ping River in Thailand, Hydrology 10 (2023) 70. doi:10.3390/hydrology10030070.

[8] J. Chen, Y. Wang, J. Wang, Y. Zhang, Y. Xu, O. Yang, R. Zhang, J. Wang, Z. Wang, F. Lu, The Performance of Landsat-8 and Landsat-9 Data for Water Body Extraction Based on Various Water Indices: A Comparative Analysis, Remote Sensing 16 (2024) 1984. doi:10.3390/rs16111984.

[9] A. K. Shakya, A. Ramola, A. Vidyarthi, Integrated modelling of soil moisture by evaluating backscattering models Dubois, Oh and IoT sensor development for field moisture estimation,

Modeling Earth Systems and Environment 9 (2023) 3381–3402. doi:10.1007/s40808-023-01693-7.
[10] J. V. Fayne, L. C. Smith, T. H. Liao, L. H. Pitcher, M. Denbina, A. C. Chen, B. A. Williams, Characterizing Near-Nadir and Low Incidence Ka-Band SAR Backscatter From Wet Surfaces and Diverse Land Covers, IEEE Journal of Selected Topics in Applied Earth Observations and Remote Sensing 17 (2024) 985–1006. doi:10.1109/JSTARS.2023.3317502.
[11] M. A. Günen, U. H. Atasever, Remote sensing and monitoring of water resources: A comparative study of different indices and thresholding methods, Science of The Total Environment 926 (2024) 172117. doi:10.1016/j.scitotenv.2024.172117.
[12] A. H. Nguyen, P. T. Nguyen, T. T. N. Nguyen, Enhanced flood water depth estimation from Sentinel-1A images, International Journal of Remote Sensing 44 (2023) 6399–6421. doi:10.1080/01431161.2023.2268819.
[13] O. Kavats, D. Khramov, K. Sergieieva, J. Puputti, J. Joutsenvaara, O. Kotavaara, Optimal Threshold Selection for Water Bodies Mapping from Sentinel-L Images Based On Sentinel-2 Water Masks, in: Proceedings of the IGARSS 2022-2022 IEEE International Geoscience and Remote Sensing Symposium, IEEE, Kuala Lumpur, Malaysia, 2022, pp. 5551–5554. doi:10.1109/IGARSS46834.2022.9883600.
[14] O. Kavats, D. Khramov, K. Sergieieva, Surface Water Mapping from SAR Images Using Optimal Threshold Selection Method and Reference Water Mask, Water 14 (2022) 4030. doi:10.3390/w14244030.
[15] V. Y. Kashtan, V. V. Hnatushenko, Machine learning for automatic extraction of water bodies using Sentinel-2 imagery, Radio Electronics, Computer Science, Control 1 (2024) 118–127. doi:10.15588/1607-3274-2024-1-11.
[16] S. J. Valman, D. S. Boyd, P. E. Carbonneau, M. F. Johnson, S. J. Dugdale, An AI approach to operationalise global daily PlanetScope satellite imagery for river water masking, Remote Sensing of Environment 301 (2024) 113932. doi:10.1016/j.rse.2023.113932.
[17] K. Kathirvelu, A. V. P. Yesudhas, S. Ramanathan, Spectral unmixing based random forest classifier for detecting surface water changes in multitemporal pansharpened Landsat image, Expert Systems with Applications 224 (2023) 120072. doi:10.1016/j.eswa.2023.120072.
[18] S. Palabıyık, T. Akkan, Evaluation of water quality based on artificial intelligence: performance of multilayer perceptron neural networks and multiple linear regression versus water quality indexes, Environment, Development and Sustainability (2024) 1–24. doi:10.1007/s10668-024-05075-6.
[19] S. Kossieris, M. Asgarimehr, J. Wickert, Unsupervised Machine Learning for GNSS Reflectometry Inland Water Body Detection, Remote Sensing 15 (2023) 3206. doi:10.3390/rs15123206.
[20] O. Nepsha, S. Hryshko, L. Prokhorova, T. Zavialova, V. Lysenko, Environmental Consequences of the Explosion of the Kahovsky Hydroelectric Plant on Biodiversity, Revista de la Universidad del Zulia 15 (2024) 163–178. doi:10.46925//rdluz.42.09.
[21] F. Filipponi, Sentinel-1 GRD Preprocessing Workflow, Proceedings 18 (2019) 11. doi:10.3390/ECRS-3-06201.
[22] A. A. Lydia, F. S. Francis, Multi-label classification using deep convolutional neural network, in: Proceedings of the 2020 International conference on innovative trends in information technology (ICITIIT), IEEE, Kottayam, India, 2020, pp. 1–6. doi:10.1109/ICITIIT49094.2020.9071539.
[23] M. Magdin, J. Benc, Š. Koprda, Z. Balogh, D. Tuček, Comparison of Multilayer Neural Network Models in Terms of Success of Classifications Based on EmguCV, ML.NET and Tensorflow.Net, Applied Sciences 12 (2022) 3730. doi:10.3390/app12083730.
[24] K. H. Shih, C. T. Chiu, J. A. Lin, Y. Y. Bu, Real-time object detection with reduced region proposal network via multi-feature concatenation, IEEE transactions on neural networks and learning systems 31 (2019) 2164–2173. doi: 10.1109/TNNLS.2019.2929059.

[25] F. Wagner, A. Eltner, H.G. Maas, River water segmentation in surveillance camera images: A comparative study of offline and online augmentation using 32 CNNs, International Journal of Applied Earth Observation and Geoinformation 119 (2023) 103305. doi:10.1016/j.jag.2023.103305.
[26] V. Khilchevskyi, V. Grebin, S. Dubniak, M. Zabokrytska, H. Bolbot, Large and small reservoirs of Ukraine, Journal of Water and Land Development 52 (2022) 101–107. doi:10.24425/jwld.2022.140379.
[27] V. I. Vyshnevskyi, S. A. Shevchuk, The Impact of the Kakhovka Dam Destruction on the Water Temperature in the Lower Reaches of the Dnipro River and the Former Kakhovske Reservoir, Journal of Landscape Ecology 17 (2024) 1–17. doi:10.2478/jlecol-2024–0008.
[28] R. Novitskyi, H. Hapich, M. Maksymenko, V. Kovalenko, Loss of fisheries from destruction of the Kakhovka reservoir, International Journal of Environmental Studies 81 (2024) 315–323. doi:10.1080/00207233.2024.2314890.
[29] A. Gulácsi, F. Kovács, Sentinel-1-Imagery-Based High-Resolution Water Cover Detection on Wetlands, Aided by Google Earth Engine, Remote Sensing 12 (2020) 1614. doi:10.3390/rs12101614.